Supplemental information for the paper:
Effects of thermal rippling on the frictional properties of free-standing graphene
by A. Smolyanitsky

S1. Thermally activated friction

In the theory of thermally activated friction, temperature (and velocity) dependence is expressed via [1]:

$$\frac{1}{\beta k_B T}(F_{max} - F)^{3/2} = ln\frac{v_0}{v} - \frac{1}{2}\ln\left(1 - \frac{F}{F_{max}}\right), \quad \text{(S1)}$$

where F_{max} is the lateral force amplitude at 0 K, v_0 is as defined in the main text with a fitting parameter $f_0 \sim \frac{1}{2\pi}\left(\frac{k}{m_{tip}}\right)^{1/2}$ ($k = \frac{k_0 k_1}{k_0 + k_1}$, where $k_0 = 1.53\ N/m$, and $k_1 = 10\ N/m$ are the first derivative of the lateral force with respect to the sliding distance (Fig. S2) and the virtual cantilever lateral stiffness, respectively) at a given normal load for a tip with an effective mass m_{tip}, and $\beta = \frac{3\pi\sqrt{F_{max}}}{2\sqrt{2}a}$ [1]. Note that the average friction force in Eq. S1 is equal to the lateral force amplitude *F*, which assumes overrelaxation of the tip-sample contact. Here (and often experimentally) the actual friction force F_f (lateral force offset, also see section below) is only a fraction of F with $\alpha = F_f/F$ corresponding to the overall dissipative properties of the experimental or simulated system.

For a light CNT tip comprised of approximately 200 carbon atoms, $m_{tip} = 4 \times 10^{-24}\ kg$, which, with $k = 1.5\ N/m$ yields $f_0 = 97.6\ GHz$.

Given the values of f_0 and *k* obtained above, we obtain $v_0 = 2.54\ m/s$. Again, one should note that the value of k_0 (and thus f_0) in general are not constant, depending on the amplitude of the lateral force as a function of sliding distance (Fig. S2), making these values load-dependent.

We solved Eq. (S1) numerically for *F* and report here F_f, using the lateral force amplitudes and the values of α at 2 K as taken directly from the simulated data; f_0 was the only fitting parameter. The results are shown in Fig. S1 for $v = 1\ m/s$. In particular, no increasing trends with respect to temperature are observed in a general sweep of f_0 (Fig. S1 (b)) and *no Eq. (S1) solutions were found for* $f_0 < 4\ GHz$.

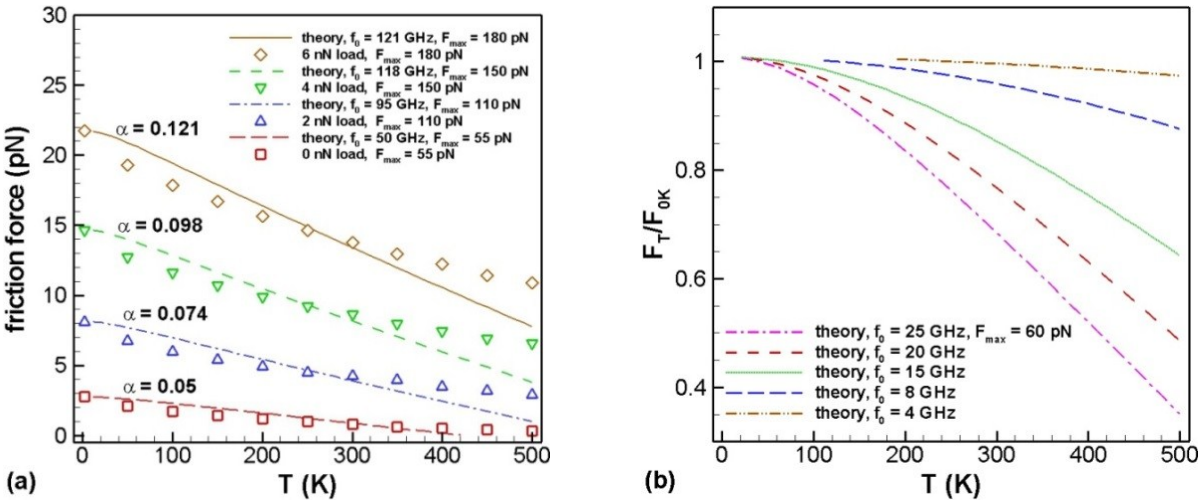

Figure S1. Comparison between simulated data and existing theory for the supported sample at all simulated normal loads (a); a sweep of f_0 for a typical F_{max} value obtained from simulations (b).

S2. Friction force calculation

The high computational efficiency of the harmonic constraints enabled us to simulate 10 ns of scanning (unless stated otherwise), providing good statistics in terms of the number of lateral stick-slip events experienced by the tip. All force averages were calculated during the last 7.5 ns of each simulation. The mean friction forces presented in the main text were calculated as averages of the lateral force trace data (with a total simulated bandwidth of 250 THz, as dictated by the time-step of 1 fs and the rate of tip-sample force output of every 20 time-steps). A low-pass filter was applied to the raw lateral force data in order to remove added high-frequency thermal noise prior to calculating averages. The effective bandwidth of the filter was 20 GHz, while the characteristic stick-slip frequency corresponded to 4 GHz (at the tip highest sliding velocity of 1 m/s). The grand averages were calculated from the per-bin averages, as described in Fig. S2.

The stick-slip periodicity necessary for combining the data accurately into bins was calculated directly from the Fourier transform peak of the lateral force data, as shown in the inset of Fig. S2. The use of bins was dictated by the fact that the absolute value of the sought average (offset) is about an order of magnitude smaller than the (locally varying) lateral force amplitude (see values of α in Fig. S1 (a)). In addition, the periodicity of the lateral force is distributed over a distance of about 0.15 Å, as shown in the inset of Fig. S2, contributing to the overall variation of local average between the stick-slip events.

Throughout the presented average friction data, the relative standard deviation varied from 1 % at the temperature of 2 K to 13 % at 500 K.

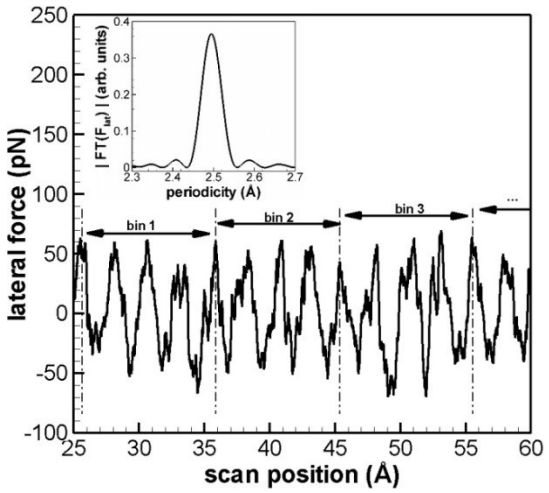

Figure S2. Calculation of average friction from lateral force data (from 0 nN normal load, 300 K of Fig. 2 (a) of main text) with use of data bins. The inset shows the Fourier spectral density of the lateral force data presented; the position of the peak is the effective lattice constant of the scanned sample λ. The width of each bin is an integer number of λ. All lateral scans were performed along the *negative* direction of the Y-axis, resulting in a *positive* average.

S3. Graphene model

The computationally efficient graphene representation used in this work is an extension of the approach presented [2] and used earlier [3-6], based on a generic model in molecular mechanics [7, 8]. The model was described in detail and dynamically tested in [9] using Nosé-Hoover thermostatics.

For this work, the stiffness constants $k_{bond} = \frac{\partial^2 V_{ij}}{\partial r^2} = 698.13\ N/m$, $k_{ang} = 2\frac{\partial^2 V_{ij}}{\partial cos\theta^2} = 8.08\ eV$, $k_{dih} = \frac{\partial^2 V_{ij}}{\partial \alpha^2} = 0.360\ eV/rad^2$ [9]. The used model is mathematically guaranteed to yield 0 K structural properties of graphene in agreement with the "parent" bond-order potential for small isotropic strains [2]. In addition to the previously published validation of the approach, we specifically tested our harmonic constraint model against the "parent" optimized second-generation bond-order Brenner potential [10] by directly simulating the thermal rippling process using both methods and calculating the time-averages of the effective ripple height $\langle h^2 \rangle^{1/2}$, thermostatted with use of the Langevin scheme along the sample perimeter, as used in this work. The results of the comparison are shown in Fig. S3, as calculated for a 8192-atom graphene sample with full periodic boundary. The rippling magnitudes (and thus the effects thereof, as reported in the main text) are somewhat *underestimated* by the harmonic constraint model, compared to the optimized Brenner potential, arising primarily from higher-amplitude modes at $q < 0.2$ Å^{-1} ($\lambda > 3.1$ nm) in the latter (see inset). The differences between the two models increase with increasing temperature. Such increasing discrepancy is natural, because agreement is only expected near 0 K, as follows from the constraint energy form used [9]. Nevertheless, the order of magnitude of the simulated rippling heights for both models is qualitatively consistent with the fundamental theory of thermally fluctuating membranes [11], as well as with previously published work [6, 12, 13].

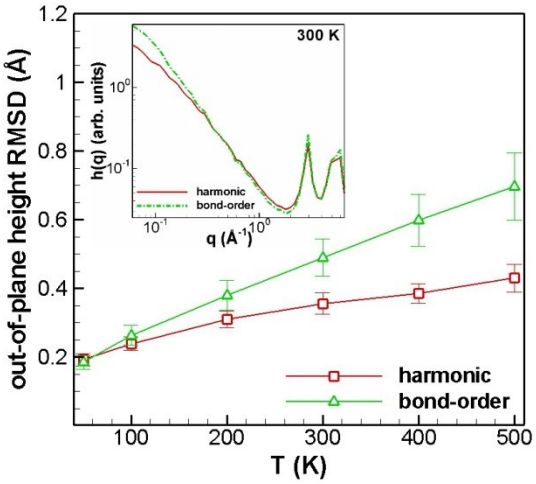

Figure S3. Out-of-plane height RMSD as a function of temperature for the 8192-atom graphene sample. The bars represent the time-variance of the calculated RMSD. The inset shows spatial distributions of the out-of-plane ripples at T = 300 K.

S4. Scaling and lateral strain

The effects of scaling are shown in Fig. S4, where in (a) we plot the friction force as a function of temperature for various sample sizes at 0 nN normal load. The differences in $\left(\frac{dF}{dT}\right)$ trends, as well as in the rippling distributions (see inset) are observed, depending on size, demonstrating high sensitivity of $\left(\frac{dF}{dT}\right)$ on the sample size. This indeed includes possible effects of anharmonic coupling, manifested by local decreases in distribution slopes at $q < 0.2$ Å^{-1} ($\lambda > 3.1$ nm), depending on sample size (top left of inset), as mentioned in the main text and consistent with [6]. Additionally, differences in the Bragg peak heights (especially the second peak) are also observed (bottom right of inset), which directly affects the thermal activation mechanism *b(T)*. In Fig. S4 (b), we examine the effect of lateral strain: a $\left(\frac{dF}{dT}\right) > 0$ trend is observed below 100 K for the strained sample, in contrast with the strain-free case. As shown in the inset, rippling is suppressed overall as a result of strain. Importantly, the local distribution slope is modified significantly throughout $q < 1.0$ Å^{-1} ($\lambda > 0.63$ nm), as expected from pre-stretching a membrane [11]. The first Bragg peak in the inset is also suppressed, again likely contributing to *b(T)*.

All rippling distributions were averaged over a 1000 sets of Fourier data from atomic position snapshots.

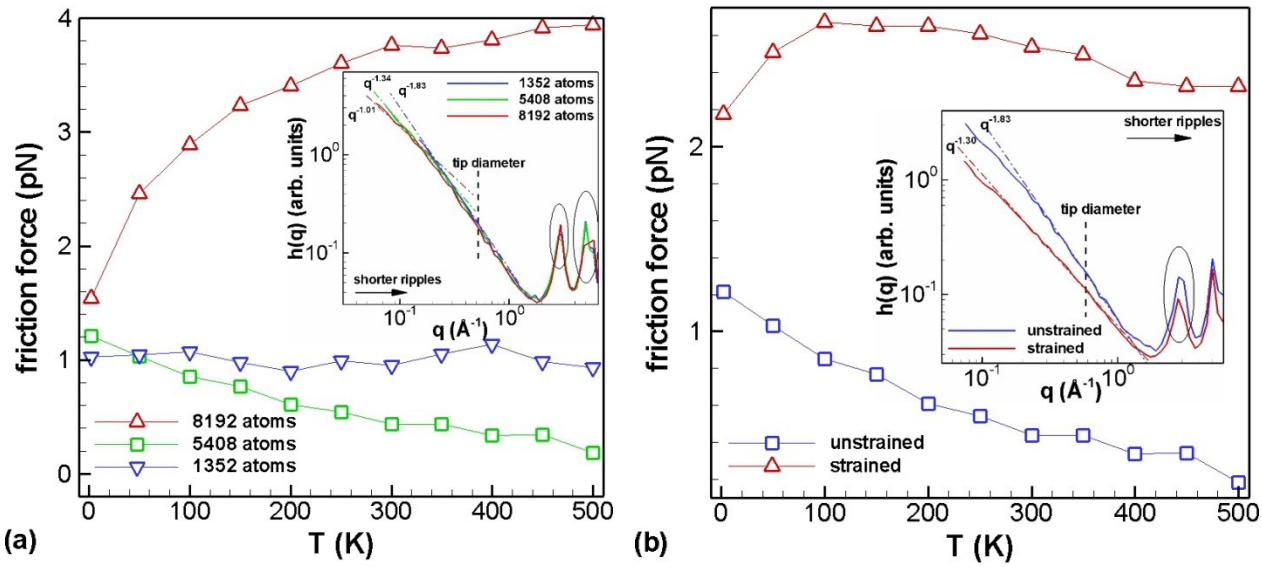

Figure S4. Friction as a function of temperature for different sample sizes at 0 nN normal load; inset shows the *h(q)* distributions obtained from the snapshots of atomic positions at T = 300 K (a); friction as a function of temperature at 0 nN normal load for a 5408 sample without strain and with 1.3 % lateral strain.

S5. Simulation and theory comparison

Although the theoretical discussion presented in the main text is qualitative, in Fig. S5 we show the data set from Fig. 4 (a) alongside the corresponding fits of Eq. (5). Here, we assume that the *functional form* of Eq. (S1) is unaffected by the presence of waves in free-standing samples, and thus the (1- *b(T)*) portion of Eq. (5) is solved directly with use of Eq. (S1). The effects of waves on the actual physics (within the assumed Tabor-like model) are then accounted for by the values f_0 and ε, used as fitting parameters.

The values of F_{max} for the 1.2 nm and 2.2 nm tip were taken directly from simulation and are equal to 60 pN and 100 pN, respectively. The values of f_0 were set to 8 GHz and 20 GHz for the 1.2 nm and 2.2 nm wide tip, respectively. With such values of f_0, the *b(T)* << 1 hypothesis for the free-standing samples is indeed supported (see Fig. S1 (b) above). One notes that the increase of f_0 for the 2.2 nm wide tip (relative to the 1.2 nm tip) makes qualitative sense, as the lateral stick-slip amplitude increases with the tip diameter. The fitting values of ε are shown in Fig. S5.

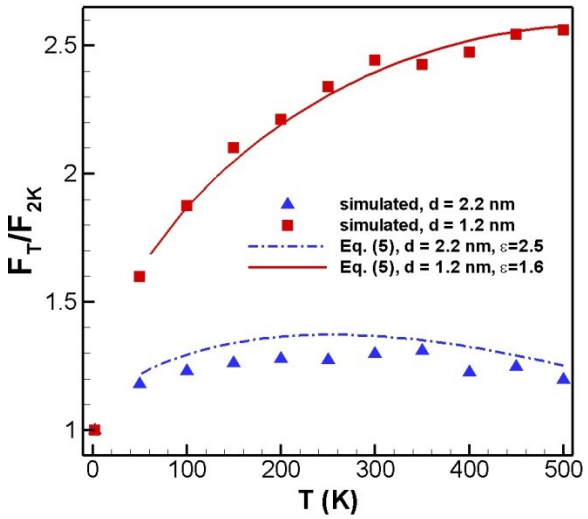

Figure S5. Data from Fig. 4 (a) alongside corresponding Eq. (5) fits. The continuous lines are shown only for temperatures, where the solution of Eq. (S1) was found.

References

1. Riedo, E., et al., *Interaction Potential and Hopping Dynamics Governing Sliding Friction.* Physical Review Letters, 2003. **91**(8): p. 084502.
2. Shakouri, A., T.Y. Ng, and R.M. Lin, *A new REBO potential based atomistic structural model for graphene sheets.* Nanotechnology, 2011. **22**(29): p. 295711.
3. Kauzlarić, D., et al., *Markovian dissipative coarse grained molecular dynamics for a simple 2D graphene model.* The Journal of Chemical Physics, 2013. **137**(23): p. 234103.
4. Zhu, S., Y. Huang, and T. Li, *Extremely Compliant and Highly Stretchable Patterned Graphene,.* Applied Physics Letters, 2014. **104**(18).
5. Smolyanitsky, A., et al., *Effects of surface compliance and relaxation on the frictional properties of lamellar materials.* RSC Advances, 2014. **4**(51): p. 26721-26728.
6. Los, J.H., et al., *Scaling properties of flexible membranes from atomistic simulations: Application to graphene.* Physical Review B, 2009. **80**(12): p. 121405.
7. Apol, E., et al., *GROMACS 4.5.6 manual*. 2010.
8. Mayo, S.L., B.D. Olafson, and W.A. Goddard, *DREIDING: a generic force field for molecular simulations.* The Journal of Physical Chemistry, 1990. **94**(26): p. 8897-8909.
9. Smolyanitsky, A., *Molecular dynamics simulation of thermal ripples in graphene with bond-order-informed harmonic constraints.* Nanotechnology, 2014. **25**(48): p. 485701.
10. Lindsay, L. and D.A. Broido, *Optimized Tersoff and Brenner empirical potential parameters for lattice dynamics and phonon thermal transport in carbon nanotubes and graphene.* Physical Review B, 2010. **81**(20): p. 205441.
11. Nelson, D., S. Weinberg, and T. Piran, eds. *Statistical Mechanics of Membranes and Surfaces*. 2 ed. 2004, World Scientific: Singapore.
12. Fasolino, A., J.H. Los, and M.I. Katsnelson, *Intrinsic ripples in graphene.* Nature Materials, 2007. **6**(11): p. 858 - 861.
13. Smolyanitsky, A. and V.K. Tewary, *Manipulation of graphene's dynamic ripples by local harmonic out-of-plane excitation.* Nanotechnology, 2013. **24**(5): p. 055701.